Durability Characterization of Mechanical Interfaces in Solar Sail Membrane Structures

Jin Ho Kang[a,*], Keith Gordon[b], Robert Bryant[c], Olive Stohlman[d], W. Keats Wilkie[d], Amanda Stark[e], Randall Barfield[f], Benjamin Sindle[g], Miria Finckenor[i] and Paul Craven[i]

[a]*National Institute of Aerospace, Hampton, VA, USA*
[b]*Advanced Materials and Processing Branch, NASA Langley Research Center, Hampton, VA, USA*
[c]*Durability, Damage Tolerance and Reliability Branch, NASA Langley Research Center, Hampton, VA, USA*
[d]*Structural Dynamics Branch, NASA Langley Research Center, Hampton, VA, USA*
[e]*Structural and Thermal System Branch, NASA Langley Research Center, Hampton, VA, USA*
[f]*NASA Langley Intern Student, University of Florida, Gainesville, FL, USA*
[g]*NASA Langley Volunteer Student, Virginia Polytechnic Institute and State University, Blacksburg, VA, USA*
[i]*Nonmetallic Materials and Space Environmental Effects Branch, NASA George C. Marshall Space Flight Center, Huntsville, AL, USA*

Abstract

The construction of a solar sail from commercially available metallized film presents several challenges. The solar sail membrane is made by seaming together strips of metallized polymer film. This requires seaming together a preselected width and thickness of a base material into the required geometry, and folding the assembled sail membranes into a small stowage volume prior to launch. The sail membranes must have additional features for connecting to rigid structural elements (e.g., sail booms) and must be electrically grounded to the spacecraft bus to prevent charge build up. Space durability of the material and mechanical interfaces of the sail membrane assemblies will be critical for the success of any solar sail mission. In this study, interfaces of polymer/metal joints in a representative solar sail membrane assembly were tested to ensure that the adhesive interfaces and the fastening grommets could withstand the temperature range and expected loads required for mission success. Various adhesion methods, such as surface treatment, commercial adhesives, and fastening systems, were experimentally evaluated and will be discussed.

Keywords: Solar sail membrane, Polymer, Metal, Interface, Adhesion

Nomenclature

λ	Wavelength (nm)
α	Absorptance (dimensionless quantity)
ε	Emittance (dimensionless quantity)
σ	Reflectance (dimensionless quantity)
τ	Transmittance (dimensionless quantity)

Subscripts

S	Solar
T	Thermal

1. Introduction

Solar sails are attractive spacecraft propulsion systems that offer extended mission capability by deriving thrust directly from momentum transfer of solar photons, rather than on-board propellant [1-2]. The transferred photon momentum is very small but the acceleration can be maximized by increasing the surface area of the sail, and reducing the overall system mass. Since sizes of commercially available metallized polymer membranes are limited, it is necessary to seam together preselected widths and thicknesses of a base material into the required sail membrane geometries. The assembled sail membranes must then be folded and stowed within small volumes prior to launch. Ensuring proper adhesion at the interfaces of the assembled sail

* Corresponding author, jin.h.kang@nasa.gov

film membranes throughout the entire mission lifecycle, including assembly, packaging, launch, deployment, and mission operations, is essential for overall mission success.

Silicone adhesive or pressure sensitive adhesive transfer tape has been widely used as a seaming method in space applications [3-7]. However, silicone adhesive requires a long period for cure, extra effort to control uniform thickness and appropriate ventilation during application due to the toxicity of uncured chemicals [3-4]. In addition, silicone is degraded into low molecular weight (LMW) cyclic silicones by space radiation [5-6], which can contaminate the reflective surface in the form of silicon dioxides, resulting in reduced reflectivity. The pressure sensitive adhesive transfer tape is easy to use and non-toxic. However, adhesion strength shows a large temperature dependency (50% decrease with a temperature increase of 70°C) [7], and the edge of the adhesive tape can rupture the sail membrane during assembly, folding, and deployment if it inadvertently adheres to adjacent sail membrane areas.

Polyester-based hot-melt web adhesive has been widely used in textile industries because of its ease of use, quick application, broad usage temperature, the absence of sticking issues after application, and good thickness control [8]. Although the packing efficiency of the sail membrane can be improved, there has been no systematic study for the solar sail application.

This study investigated the different interfaces of metallized coating-to-polymer (or metallized/polymer) joints of sail structures including metallized/sail membrane and metallized/seaming adhesive joints. Optical and adhesion properties of a metallized sail membrane are characterized. A new seaming technology using the hot-melt web adhesive was demonstrated, and the adhesion strength was evaluated at a broad range of test temperatures for the simulated space environment. A quantitative study of the adhesion strength can provide guidelines to increase the reliability of seamed solar sail structures.

2. Experimental

2.1. Materials

In this study, metallized polyethylene naphthalate (PEN) films were used as a baseline representative solar sail membrane material. The core membrane material was purchased from Dupont Teijin (Teonex® Q72, 2 μm thick). The PEN core material was metallized via magnetron sputtering of aluminum (100 nm) on one side of the membrane (which serves as reflective layer) and chromium (15 nm) on the opposite side (which serves as a thermal emittance layer for passive cooling). Metallization was performed by Astral Technology Unlimited, Inc., MN, USA. Samples of chromium and aluminum at various thicknesses were also prepared for optical properties and mechanical adhesion testing. Metallization of these samples was performed via thermal evaporation (Edward auto 306 FL400 thin film deposition system).

Several additional metallized sail materials were also evaluated in this study. The additional materials included in this study were aluminized polyethylene terephthalate (PET, Mylar®, Dupont, 2.54 μm), aluminized LaRC™ CP1 polyimide (CP1, 2.54 μm), and metallized polyimide (PI, Kapton® EN, 5 μm). Both aluminized PET and aluminized LaRC™ CP1 polyimide consisted of an aluminum layer (90 nm) deposited by e-beam evaporation. The metallized polyimide consisted of an aluminum (100 nm) layer on the front side of the membrane (the reflective layer) and chromium (30 nm) on the back side of the membrane (the thermal radiation layer). The aluminized PET material was purchased from SteinerFilm, Inc. (MA, USA). The aluminized LaRC™ CP1 polyimide (2.54 μm) was purchased from NeXolve Co. (AL, USA) and the metallized polyimide (Kapton® EN, 5 μm) was obtained from Astral Technology Unlimited, Inc. (MN, USA).

Two polyester based hot-melt adhesives, PA 1811 (24 g/m^2, SpubFab Ltd, OH, USA) and PE 165 (14.5 g/m^2, Bostik Co., France) were evaluated for the solar sail seaming process.

2.2. Characterization

The thermo-optical properties [thermal emittance (ε_T), thermal reflectance (ρ_T), thermal transmittance (τ_T), solar absorptance (α_S), solar reflectance (ρ_S) and solar transmittance (τ_S)] were measured using a portable emissometer (TEMP 2000, AZ Technology, AL, USA) and a laboratory portable spectroreflectometer (LPSR 300, AZ Technology, AL, USA).

The adhesion strength of aluminum/PEN (or aluminum/chromium/PEN) joints was characterized by a T-peel adhesion test (ASTM D1876). Plasma treatment was performed under air plasma for 30 minutes using XEI Scientific Evactron® Model 25. The radio frequency (RF) plasma power was measured at 20 J/s and the chamber pressure was 53 Pa. The thickness of the PEN membrane (2 μm) required an adhesive [poly(ethylene-co-methacrylic acid)] coated aluminum foil tape (~100 μm thick, Western Plastics, CA, USA) as backing material to create the sandwich structure, 10 mm wide and 90 mm long, shown in Fig. 1. A strip of Teflon™ film was inserted between the PEN and adhesive layer to serve as a crack initiation point. This sandwich was placed in a hot press for about 7 minutes

at 204°C using a pressure range of 80-100 kPa to create the T-peel specimen.

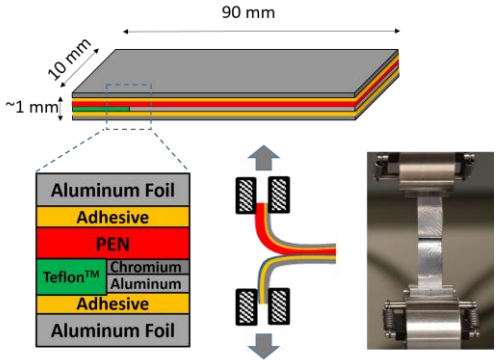

Fig. 1. Adhesion strength test specimen for metal/PEN joints (T-peel adhesion test, ASTM D1876).

Adhesion strength of the seamed solar sail membrane joints using the hot-melt web adhesive was characterized according to a modified ASTM standard D5868. Because of the current sail membrane seaming design, the 12.7 mm × 9.5 mm overlap (adhesive size) was employed instead of the standard 25.4 mm × 25.4 mm overlap for the test. The hot-melt web adhesive was placed between the aluminum (Al) side of sail membrane and chromium side (Cr) of sail membrane. The test specimen and test fixture are shown in Fig. 2.

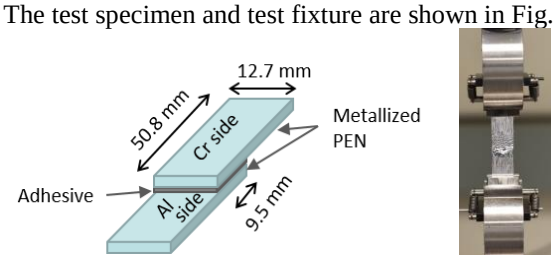

Fig. 2. Lap shear test specimen of the seamed solar sail membrane.

A Hitachi S-5000 high-resolution scanning electron microscope (HSEM), equipped with a field emission electron gun and in-lens detector, was used to examine the surface morphology of the metallized PEN film. The locus of failure was evaluated by element analysis using energy dispersive X-ray spectrometry (EDS, EDAX Inc., NJ, USA).

The thermal properties of melting, crystalline and glass transition temperature of the metallized PEN film were characterized at a heating rate of 3°C/min and thermally cycled at ±0.47°C/min using a modulated differential scanning calorimeter (MDSC, Q20, TA Instruments, DE, USA). Thermal stability of the hot-melt adhesives was characterized at a heating rate of 10°C/min and air atmosphere using a thermogravimetric analyser (TGA, Q50, TA Instruments, DE, USA).

3. Results and Discussion

3.1. Candidate Sail Materials for NASA solar sails

Membrane structures and optical properties of the candidate solar sail materials are summarized in Tables 1-3. Kapton® EN polyimide, was selected as a sail membrane for the Sunjammer project [9]. It has relevant thermal and mechanical properties and is an excellent candidate material for the harsh space environment. The film has a reflective aluminum layer (100 nm, $\rho_S \sim 0.9$) on the front side, and chromium (30 nm, $\varepsilon_T \sim 0.48$) on the back side for passive cooling. However, an ultrathin film is not commercially available due to a manufacturing limit (>5 μm). Compared to the Kapton® EN polyimide, LaRC™ CP1 polyimide (colorless polyimide) has less yellow or tan color, due to charge transfer between the fluorinated polymer backbones. The solubility of LaRC™ CP1 polyimide allows for membrane fabrication as thin as 2.54 μm via solution casting. However, the high cost of the LaRC™ CP1 polyimide is a major obstacle in expanding its applications. The aluminized LaRC™ CP1 is considered for use for the near-earth asteroid (NEA) scout project. Commercial polyester thin membrane materials such as PET and PEN film can also be acceptable low-cost sail material candidates for some mission applications. Ultra-thin polyester membrane (~0.9 μm) is commercially available in continuous rolls for electronic component manufacturing, such as thin film capacitors, and costs about 100 times less than LaRC™ CP1 polyimide. Aluminized PET or metallized PEN membrane are candidate sail membranes for the NASA Advanced Composite Solar Sail System (ACS3) project [10]. A chromium layer (15 nm, $\varepsilon_T \sim 0.60$) was coated on the back side of the metallized PEN membrane for passive cooling.

Table 1. Candidate sail membrane materials for recent NASA solar sail projects.

Material ID	Sail Structure (material / thickness)			Comment
	Reflective Coating	Core Polymer	Emissive Coating	
Metallized PI	Al / 100 nm	Kapton® EN / 5 μm	Cr / 30 nm	Sunjam-mer
Aluminized CP1	Al / 90 nm	LaRC™ CP1 / 2.54 μm	No coating	NEA Scout
Aluminized PET	Al / 100 nm	PET / 2.54 μm	No coating	ACS3
Metallized PEN	Al / 100 nm	PEN / 2 μm	Cr / 15 nm	ACS3

Table 2. Solar optical properties of candidate sail membranes (λ_s: 250 ~ 2800 nm).

Material ID	Side	α_S	ρ_S	τ_S
Metallized PI	Al	0.10	0.90	0.00
	Cr	0.54	0.46	0.00
Aluminized CP1	Al	0.10	0.90	0.00
	CP1	0.17	0.83	0.00
Aluminized PET	Al	0.09	0.91	0.00
	PET	0.14	0.86	0.00
Metallized PEN	Al	0.10	0.90	0.00
	Cr	0.57	0.43	0.00

Table 3. Thermal infrared properties of candidate sail membranes (λ_T: 3 ~ 30 μm).

Material ID	Side	ε_T	ρ_T	τ_T
Metallized PI	Al	0.03	0.97	0.00
	Cr	0.48	0.52	0.00
Aluminized CP1	Al	0.03	0.97	0.00
	CP1	0.29	0.71	0.00
Aluminized PET	Al	0.02	0.98	0.00
	PET	0.25	0.75	0.00
Metallized PEN	Al	0.03	0.97	0.00
	Cr	0.60	0.40	0.00

3.2. The effect of chromium layer thickness on optical properties of sail membranes

The equilibrium temperature of solar sail membrane exposed to sunlight in space is, to first order, determined by the α_S and ε_T of the membrane surfaces. The ε_T of the non-sun facing side has the largest effect on the temperature of the sail by thermal radiation (passive cooling). Thus, it is important to examine the effect of the chromium coating thickness on the ε_T. Chromium layers with different thickness (7.5 ~ 25 nm) were deposited on the aluminized PET membrane samples (Table 1) by thermal evaporation. Fig. 3 shows the ε_T and ρ_T of the chromium side as a function of the chromium thickness. The ε_T of PET side (no chromium) was 0.26, and increased with increasing chromium coating thickness, 0.47 for 7.5 nm thick chromium, and 0.62 for 20 nm thick chromium. Over 20 nm in thickness, the ε_T of chromium side did not exhibit further increase and slightly decreased at 25 nm thickness. The ε_T of 12.5 nm thick chromium showed an unexpected drop from the trend, and a further investigation is ongoing. The ε_T of chromium side showed a trend opposite that of the ε_T of chromium as the transmittance was near zero.

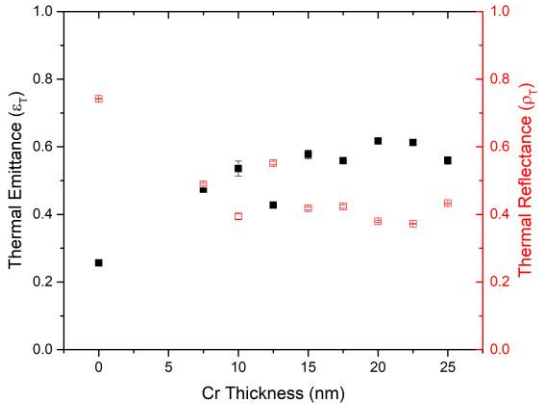

Fig. 3. The effect of chromium thickness on ε_T and ρ_T of chromium surface of the Al (100 nm)/PET (2.54 μm)/Cr sail membrane.

The ε_T (~ 0.02) and ρ_T (~ 0.98) of the aluminum layer did not change with the thickness of the chromium layer. This is because the aluminum layer, at 100 nm, is completely opaque, and the optical properties of the aluminum side are not affected by the chromium surface on the opposite side (Fig. 4).

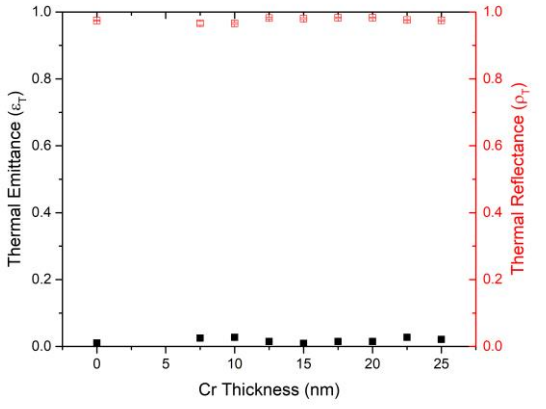

Fig 4. The ε_T and ρ_T of aluminum surface of the Al (100 nm)/PET (2.54 μm)/Cr sail membrane.

The effect of the chromium thickness on the optical properties of the metallized PEN sail membrane was investigated (Fig. 5). Different thicknesses of chromium and aluminum were deposited on the raw PEN membrane by thermal evaporation. The trend was similar to the metallized PET sail membrane. The ε_T of PEN side (no chromium) was 0.28, and it increased with increasing chromium thickness (ε_T ~ 0.51 for 7.5 nm thick chromium and ε_T ~ 0.67 for 20 nm thick chromium). Over 20 nm in thickness, the ε_T of chromium showed a slight decrease (for 25 nm thick chromium, $\boldsymbol{\varepsilon_T}$ ~ 0.61).

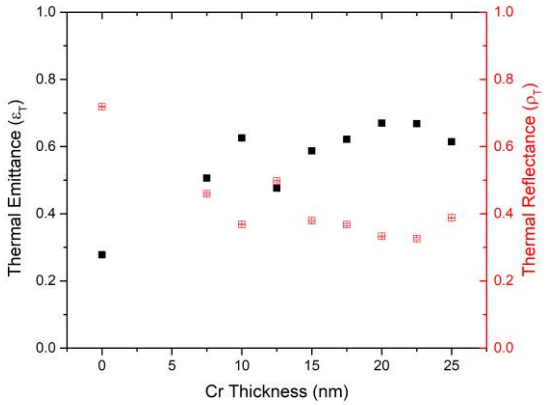

Fig. 5. The effect of chromium thickness on ε_T and ρ_T of chromium side of the Al (100 nm)/PEN (2 μm)/Cr sail membrane.

The ε_T (~ 0.04) and ρ_T (~ 0.95) of the aluminum layer did not change with the different chromium layer because of near zero transmittance through the thick aluminum layer (Fig. 6).

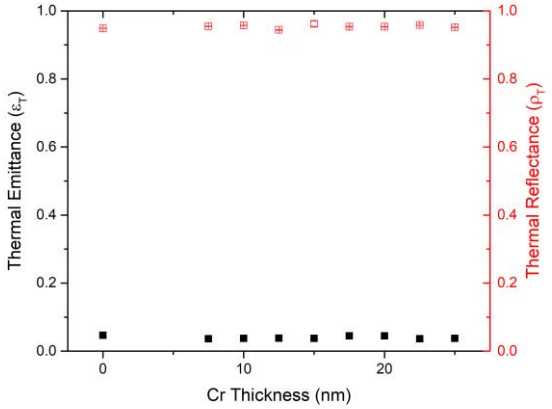

Fig. 6. The ε_T and ρ_T of aluminum layer, Al (100 nm)/PEN (2 μm)/Cr sail membrane.

3.3. Thermal Analysis of sail membranes in low Earth orbit

Because PEN shows better thermal and mechanical durability than PET, the PEN membrane was selected for the further study [11]. Thermal environmental analysis of the baseline ACS3 metallized PEN membrane (Al/PEN/Cr) was calculated using Thermal Desktop 6.0 Patch 21. The sail was simulated by starting with an Autodesk drawing of the shape of the sail and then generating a finite element method (FEM) mesh of the surface. At this point thermophysical and optical properties were added. The thermophysical properties for PEN were used, and the optical properties that were used were collected directly from the corresponding side of the sail material (Tables 2-3). The analysis used a polar orbit with an inclination of 98°, the right ascension of the ascending node (RAAN) of 270°, and an altitude of 700 km. The Thermal Desktop visual representation (Fig. 7) of the polar orbit was used for this study. During a loss of attitude control, the sail will begin to tumble and experience arbitrary orientations with respect to the sun while attitude control is being re-established. Thermal analysis of on-orbit sail temperatures need to include cases where the orientation was not optimal. This resulted in four orientation cases; (i) correct orientation with aluminum coating facing sun, (ii) reversed orientation with the chromium coating facing the sun, (iii) edge to the sun with the aluminum coating point nadir, and (iv) edge to the sun with the chromium coating pointing nadir. All cases calculated temperatures of the sail quadrants over the course of one complete orbit. Thermal Desktop has a tool that will find the maximum and minimum temperature for a specific part of the model. This tool simplified identifying the maximum and minimum temperature of all four sail quadrants, with the results shown in Table 4. These temperatures were selected for determining the sail membrane adhesion testing thermal conditions.

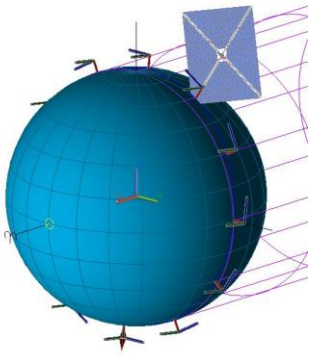

Fig. 7. Reference 700 km, 98° inclination dawn-dusk sun-synchronous polar orbit for sail thermal equilibrium analyses. The sail surface normal is perpendicular to the orbit plane. Sail is not to scale.

Table 4. The maximum and minimum temperature that the sails experience for each orientation.

Orientation	Temperatures (°C)	
	Max	Min
Al surface toward sun	4.6	0.1
Cr surface toward sun	136.5	131.0
Sail edge toward sun, Al surface toward nadir	16.4	-27.0
Sail edge toward sun, Al surface toward zenith	-16.6	-126.3

3.4. Sail membrane interfaces

Fig. 8 shows the two quadrant sail membranes fabricated by seaming metallized sail membrane material. The hypotenuse of the sail quadrant was 9.2 m.

There are several interfaces in the sail membrane: aluminum/PEN, PEN/chromium, chromium/adhesive and adhesive/aluminum. In sections 3.5 and 3.6, each interface is outlined.

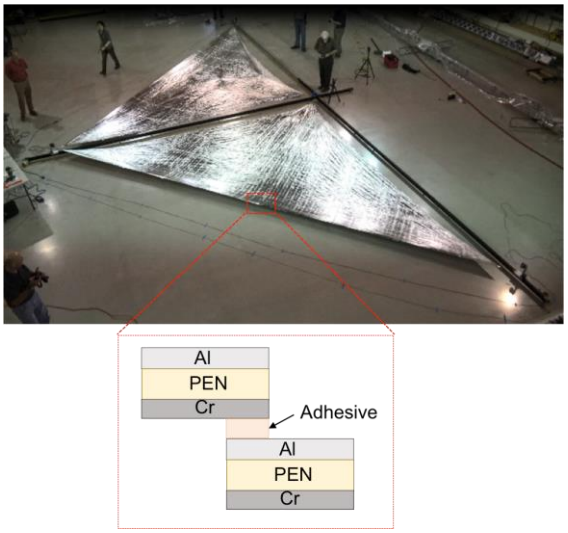

Fig. 8. Sail quadrant deployment test. The cross-sectional structure of the seamed sail membranes is shown in an inset. The edge of sail is 9.2 m.

3.5. The interfaces of between metal layers and sail core membranes

For the baseline aluminum/PEN/chromium sail material, there are two metal-to-polymer interfaces: the aluminum/PEN and chromium/PEN interfaces. Compared to chromium/PEN, aluminum/PEN has weaker interfacial strength [12-13] and local delamination of the aluminum layer was observed from creasing and wear during fold/stowage. The delamination of the aluminum layer increases with moisture in laboratory atmosphere. Thus, the adhesion strength was investigated using a T-peel adhesion test (ASTM D1876, Fig. 1) and several adhesion promotion methods were tested.

The adhesion strength of baseline Al/PEN joint was 202.9 N/m (Fig. 9). The plasma treatment (20 J/s, 30 min, 53 Pa) of PEN film before deposition of aluminum layer improved the adhesion strength by 17% (238.4 N/m). The stronger interfacial strength seems to originate in the cleaning effect and the increased surface energy by creating polar components such as hydroxyl groups [14]. Thus, the plasma treatment was employed as a pre-treatment process for further tests. When a chromium layer was deposited to the plasma treated PEN as a tie-layer prior to aluminum layer deposition, further improvement of 41 to 76% (286.6 to 357.1 N/m) was achieved for 2.5 to 10 nm thick chromium tie layers. The chromium tie layer of 7.5 nm thickness showed the highest adhesion strength (357.1 N/m). However, the PEN membranes ruptured during the test (cohesive failure in adherend), the actual adhesion strength, or interfacial strength between aluminum-chromium and the PEN could be higher than the measured values as shown by the arrows on the data columns [15]. This result suggests that the plasma treatment and chromium tie layer (about 7.5 nm thick) can be a viable way to increase the adhesion strength of metallized PEN joints.

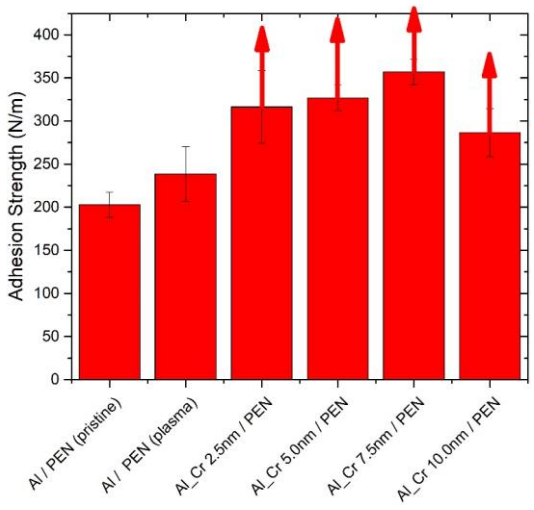

Fig. 9. Adhesion strength of aluminum/PEN and aluminum-chromium/PEN joints. Arrows indicate that the actual adhesion strength could be higher than the measured adhesion strength because cohesive failure in adherend (sail membrane) occurred.

3.6. *The interfaces of metallized PEN membranes seaming joints*

The baseline ACS3 solar sail membrane quadrant was assembled from 75 cm wide metallized PEN membrane strips or gores. Thirteen PEN membrane gores were seamed together to form a sail quadrant with a 9.2 m edge. As previously mentioned, the use of pressure sensitive adhesive creates a sticking issue. To mitigate this problem, a hot-melt adhesive was chosen as an alternative. Table 5 shows two candidate unwoven matted polyester fiber web hot-melt adhesives. While PA1811 has a melting point of 75°C, PE 165 has a higher melting point of 165°C and was selected for the seaming test in this study. The optimum condition (at least 180°C) for the hot melt process was estimated from the 1st heating run of the DSC curve, and the maximum operation temperature for long-term application was suggested from the onset point (140°C) of melting peak of the 2nd heating run (Fig. 10). Also, PE 165 has low water absorption and exhibited 5% weight loss at 340°C at a heating rate of 10°C/min (Fig. 11). Further investigation of isothermal stability is required.

Table 5. Candidate hot-melt adhesives. Note that both manufacturers produce hot-melt adhesives with a range of melting points [16-17].

Adhesive	**Weight Loss**		**Melting Point**	
	Weight loss at 110°C for 30 min	Tempera-ture at 5 wt% loss	Onset Point	Melting Peak
PA 1811	0.9 wt%	340°C	50°C	75°C
PE 165	0.4 wt%	330°C	140°C	165°C

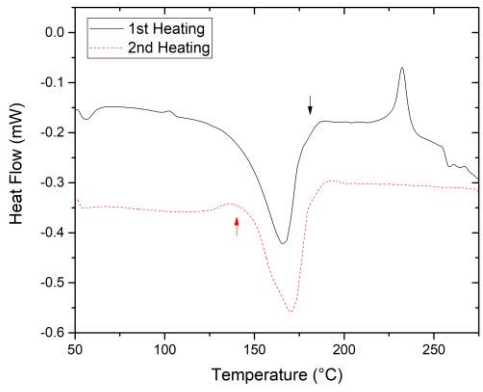

Fig. 10. Differential scanning calorimetry (DSC) curves of PE 165 nonwoven web adhesive.

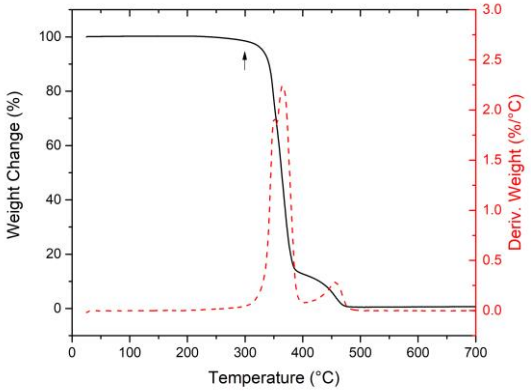

Fig. 11. Thermogravimetric analysis (TGA) of PE 165 nonwoven web adhesive.

Fig. 12 shows the seaming process. The PE 165 adhesive was cut into strips of ~ 9.5 mm) and placed on the chromium side of the metallized PEN membrane gore. The adhesive was covered by another metallized PEN gore with aluminum side down and fused with a temperature controlled iron. PEN can shrink at high temperature (0.2% at 200°C [11]), but a noticeable shrinkage was not observed.

Fig. 12. Seaming process of metallized PEN gores using PE 165 nonwoven web adhesive.

The adhesion strength seamed joint was evaluated by a modified ASTM standard D5868 lap shear test to simulate tensile loading of the adhesive joints of the deployed solar sail membrane. The test specimen and test fixture are shown in Fig. 2. Visual failures of adhesion test specimens are shown in Fig(s). 13 and 19. When the temperature of the seaming iron was below ~ 190°C, the PE 165 adhesive was not completely melted, resulting in a failure of the adhesive joint during the tensile test. As expected, the adhesive strength was weaker than the tensile strength of the metallized PEN membrane (Fig. 13). The adhesive fractured surface was investigated using a HSEM (Fig. 14). Both properly-melted web adhesive and poorly-melted web adhesive were found in the fracture surface. A small fragment of

metallized PEN membrane was found near the properly-melted adhesive area (Fig 14). Fig. 15 shows a high magnification image of properly-melted adhesive web. The surface of the web adhesive fiber was flat (Fig. 15), and chromium was found at the fracture surface of the web adhesive from the EDS analysis (Fig. 16). This indicated that there was a good contact and adhesion between the adhesive and chromium layers of the other metallized PEN membrane [15]. In comparison, the poorly-melted adhesive web showed the original round shape and unfused adhesive fibers (Fig. 17) and chromium was not found in the fracture surface of the adhesive web (Fig. 18), which indicates adhesive failure where insufficient melting occurred.

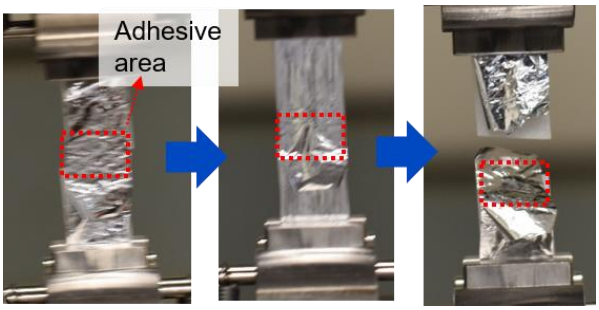

Fig. 13. An example of adhesive failure of the lap shear test specimen. The partial failure of the adhesive joint indicates generally poor or inhomogeneous adhesion.

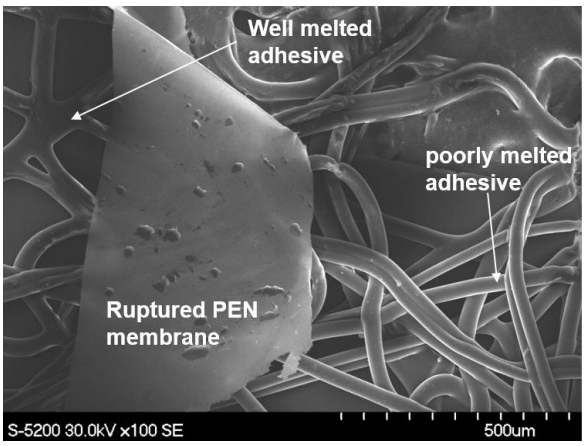

Fig. 14. HSEM image of the fracture surface of adhesive joint. Inhomogeneous melting was discovered.

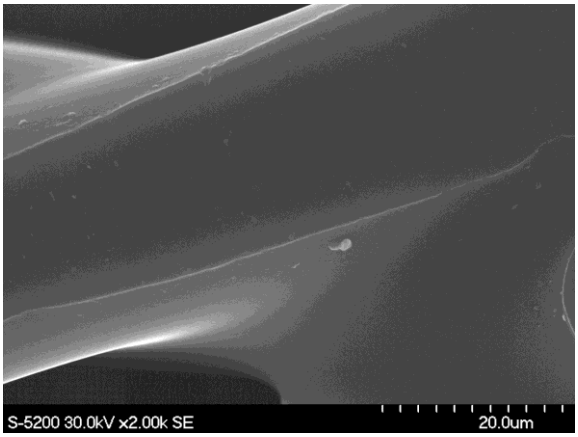

Fig. 15. HSEM image of the properly-melted PE 165 adhesive from the adhesive joint. The melted web adhesive fibers are fused and connected in a network.

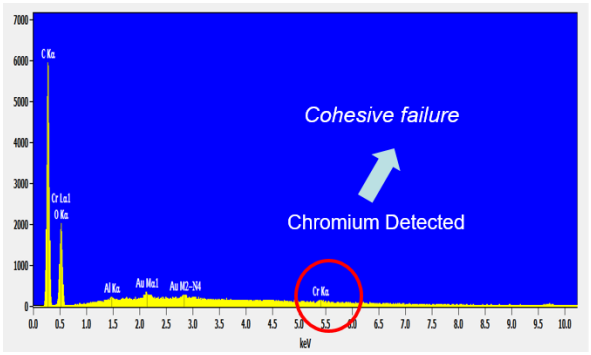

Fig. 16. Energy dispersive X-ray (EDS) Analysis of the fracture surface of properly-melted PE 165 adhesive.

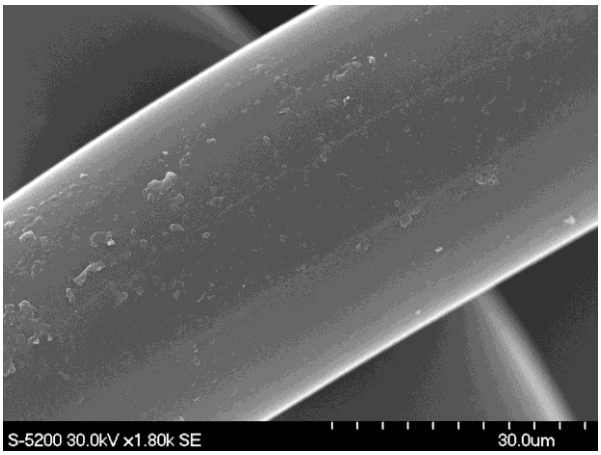

Fig. 17. HSEM image of the poorly-melted PE 165 adhesive web from the adhesive joint. The web adhesive fiber did not completely melt and fuse with other adhesive fibers.

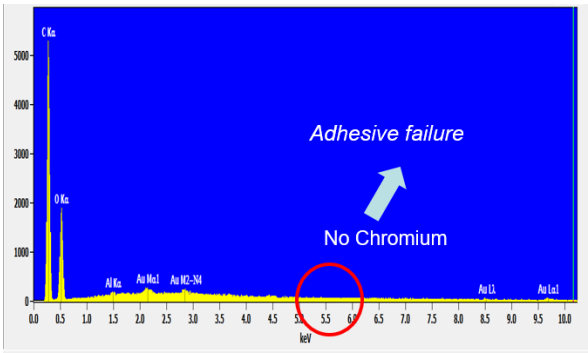

Fig. 18. Energy dispersive X-ray (EDS) Analysis of the fracture surface of poorly-melted PE 165 adhesive.

When the temperature of iron was carefully controlled to be ~ 204°C, the seamed joint displayed good adhesion strength. When the test specimen failed, the metallized PEN film was broken just above the adhesive area. Thus, the adhesion strength was higher than sail membrane (metallized PEN) tensile strength (Fig. 19).

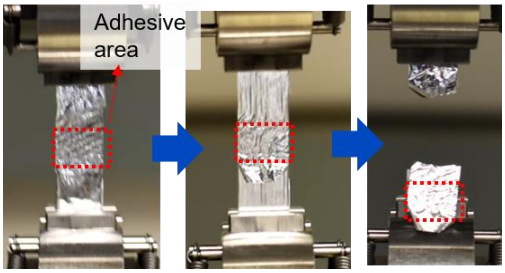

Fig. 19. An example of the adhesion test of the lap shear test specimen. The metallized PEN membrane was ruptured during test, which indicates the adhesive joint was stronger than the tensile property of the metallized PEN membrane.

From the thermal analysis of sail membrane in orbit (Section 3.3), the expected sail temperatures range from -126.3 to 136.5°C for the worst-case scenario during flight. The adhesion strength for this temperature range was evaluated. The temperature limits of the environmental oven chamber for the load frame was -70 to 200°C. The quantitative adhesion test was performed at this temperature range. A qualitative cryogenic adhesion test was performed manually by immersing the sample in a dewar flask containing liquid nitrogen (-196°C) and pulling it apart to see where the break occurred. All the specimens showed good adhesion as the membrane failed without delamination of the adhesive joint at cyrogenic temperatures.

The quantitative tensile load of the seamed joint as a function of tensile extension at different test temperatures (-70, -40, ~20, 120, 140, 160, 180, and 200°C) were recorded until the failure of the specimens (Fig. 20). From -70 to 160°C, all of the metallized PEN membranes broke before the adhesive joint failure, indicating cohesive failure of the membrane occurred. In general, acceptable adhesion was confirmed below 160°C. Above 180°C, slippage and failure of the adhesive joint occurs before cohesive failure of the membrane material due to complete melting of the PE 165 adhesive. PEN has the glass transition temperature of ~ 124°C, but both high crystallinity of PEN (~ 54%) and metal layers (aluminum and chromium) help to keep its mechanical integrity above 180°C [18]. The load at failure of the seamed joint specimens, and the failure strength normalized by the sail membrane cross-section as a function of test temperature are shown in Fig. 21. Because the adhesive strength is stronger than the tensile strength of the metallized PEN membrane, the temperature dependency of the load at failure was determined by the intrinsic tensile strength of the PEN membrane. At room temperature (~20°C), the tensile load at failure (or failure strength normalized by sail membrane cross-section) was about 4.2 N (155 MPa). Below room temperature, the load at failure decreased with decreasing temperature because the PEN membrane became less compliant (smaller elongation at break) at lower temperatures. Above room temperature, the load at failure decreased with increasing temperature because the stiffness (or modulus) of PEN membrane decreased. For all the tests, the failure strength normalized by the cross-section was higher than the estimated maximum biaxial tension level of the solar sails (~ 0.02 MPa). The apparent work of adhesion was calculated from the failure load (Fig. 22). However, the actual work of adhesion can be higher than the apparent value because cohesive failure occurred [15]. Since mixed mode failure occurred in the adhesive above 180°C, the apparent work of adhesion is approximately the same as the actual work of adhesion.

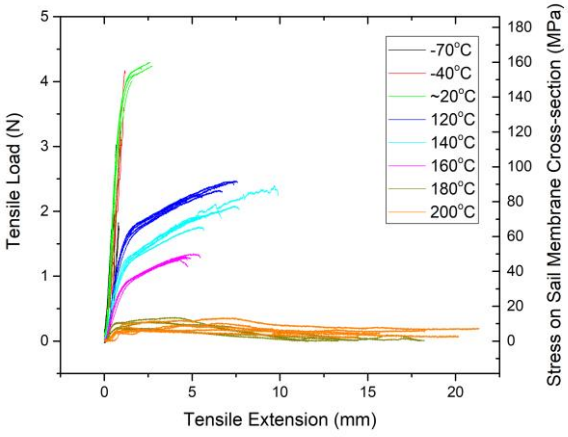

Fig. 20. Adhesion test of the seamed metallized PEN joint at temperatures from -70 to 200°C.

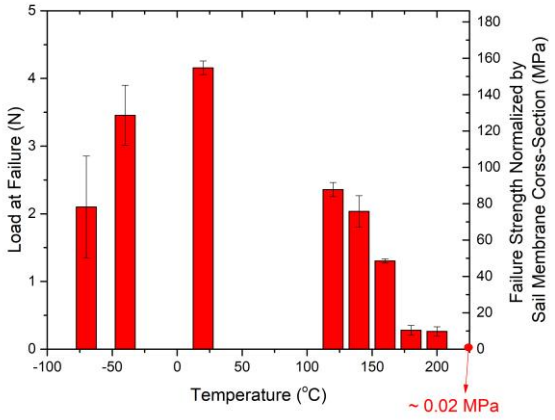

Fig. 21. Load at failure and failure strength normalized by sail membrane cross-section as a function of test temperature. Data tested at cryogenic temperature show larger deviation compared to the data tested above room temperature.

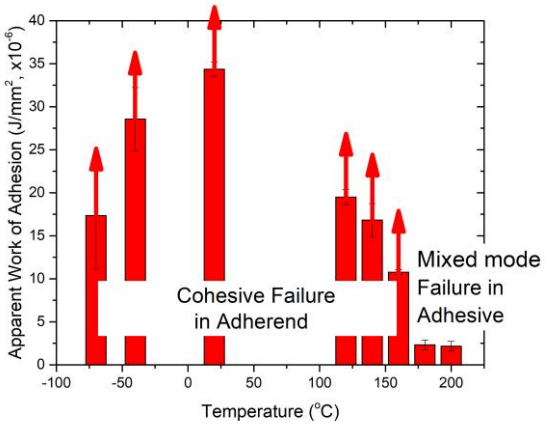

Fig 22. Apparent work of adhesion as a function of temperature. The arrows indicate that the actual work of adhesion is higher than the apparent work of adhesion because cohesive failure in adherend (sail membrane rupture) occurred. Since failure occurred in adhesive above 180°C, the apparent work of adhesion is approximately the same as the actual work of adhesion [18].

Sail quadrants were successfully fabricated utilizing the optimized seaming process obtained in section 3.6. Thirteen gores were seamed together with strips of ~ 9.5 mm wide PE 165 web adhesive [Fig. 23 (a)]. Kevlar® fiber embedded adhesive joints were used as a rip stop mechanism as needed. Once all gores were seamed together, the desired quadrant planform perimeter was drawn directly onto the sail membrane and then trimmed to the final shape [Fig. 23(b)]. Next, aluminum grommets were added to each corner. They were sandwiched with PE 165 web adhesive and the metallized PEN, and secured by heat seaming with an iron, and perforated for tip connection to booms [Fig. 23 (c-d)].

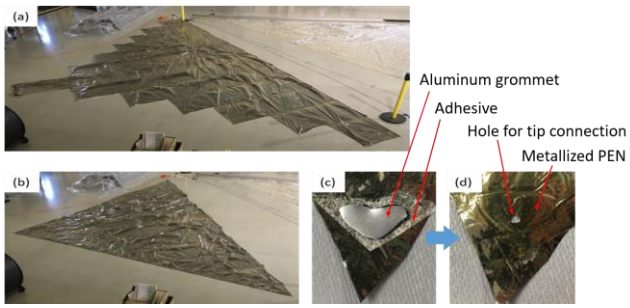

Fig. 23. A sail quadrant fabrication process. (a) seaming gores, (b) trimming, (c-d) reinforcing vertex for durable tip connection.

4. Summary

Optical properties of different solar sail membranes were characterized to estimate thermal equilibrium conditions of the sail membrane in space. The interface and adhesion of solar sail membrane structures were investigated. Adhesion strength of an aluminum and PEN membrane was improved by 17% by a plasma treatment. An additional chromium tie layer between the aluminum and the PEN membrane increased the adhesion strength by 76%. The adhesive quality of a commercial hot melt polyester web adhesive was investigated for seaming gores to fabricate sail quadrants. The seamed sail membranes with PE 165 web adhesive showed good adhesion strength over a temperature range of -196°C to 160°C, provided that optimal sealing temperatures were used. These results indicate that hot-melt adhesives are good candidate adhesives for fabricating solar sails with minimum risk of inadvertent adhesion between folds of stowed sail membranes.

5. References and Citations

[1] W.K. Wilkie, J.E. Warren, M.W. Thompson, P.D. Lisman, P.E. Walkemeyer, D.V. Guerrant and D.A. Lawrence. The Heliogyro Reloaded, Joint Army-Navy-NASA-Air Force (JANNAF) Interagency Propulsion Committee Meeting, Huntsville, AL, USA, December 5-9, 2011.

[2] C.R. Mcinnes, *Solar Sailing: Technology, Dynamics and Mission Application*, Springer Praxis, New York, 1999.

[3] C. White, K. Tan, A. Wolf and L. Carbary, Advances in structural silicone adhesives, in D. A. Dillard, editor, *Advances in Structural Adhesive Bonding*, pages 66-95, Woodhead Publishing, 2010.

[4] D.H. Filsinger. Formaldehyde levels based on bulk and elevated-temperature evolution rate measurements of silicone materials. *American Industrial Hygiene Association Journal*. 56(12): 1201-1207, 1995.
[5] F.Z. Hanrahan and N.J. Ianno. Relationship between photofixed, effluent, and bulk composition of several room-temperature-vulcanized materials. *Journal of Spacecraft and Rockets*. 51(3): 978-982, 2014.
[6] H. Xiao, C. Li and D. Yang. Optical degradation of polydimethylsiloxane under 150keV proton exposure. *Journal of Applied Polymer Science*. 109(6): 4060-4064, 2008.
[7] 3M™ adhesive transfer tape 966, https://3m.citrination.com/pif/000314 Accessed: 2019-06-05
[8] E.M. Petire. Adhesive bonding of textile: principles, types of adhesive and methods of use. In Jones, G.K. Stylios, editors, *Joining Textiels: Principles and Applications*, pages 225-274. Woodhead Publishing Series in Textiles, 2013.
[9] J. Heiligers, B. Diedrich, W. Derbes and C. McInnes. Sunjammer: Preliminary end-to-end mission design. AIAA 2014-4127, AIAA/AAS Astrodynamics Specialist Conference, San Diego, CA, August 4-7, 2014.
[10] W. Wilkie, J. Fernandez, P. Banicevic, O. Stohlman, G. Rose, J. Warren, M. Chamberlain, J. Kang, M. Straubel and J. Heiligers. An overview of NASA's advanced composite solar sail system (ACS3) low-earth orbit technology demonstration project. to be presented at the Fifth International Symposium on Solar Sailing, Aachen, Germany, July 30-August 2, 2019.
[11] W.A. MacDonald, M.K. Looney, D. MacKerron, R. Eveson, R. Adam, K. Hashimoto and K. Rakos. Latest advances in substrates for flexible electronics. *Journal of SID*. 15(12): 1075-1083, 2007.
[12] J.F. Silvain and J.J. Ehrhardt. An overview on metal/PET adhesion. *Thin Solid Film*. 236: 230-235, 1993.
[13] M.J. Cordill, A. Taylor and J. Schalko. Fracture and delamination of chromium thin films on polymer substrates. *Metallurgical and Materials Transactions A – Physical Metallurgy and Materials Science*. 41A(4): 870-875, 2010.
[14] E.M. Liston, L. Martinu and M.R. Wertheimer. Plasma surface modification of polymers for improved adhesion – a critical review. *Journal of Adhesion Science and Technology*. 7(10): 1091-1127, 1993.
[15] J.H. Kang, K. Cho and C.E. Park. Adhesion strength of poly(imide-siloxane) with alloy 42 lead frame and silicon dioxide. *Polymer*. 42: 2513-2520, 2001.
[16] Spunfab product overview, https://www.spunfab.com/product-overview/ Accessed: 2019-01-30
[17] Bostik hot melt pressure sensitive adhesive, https://www.bostik.com/smart-adhesives/lead-technologies/hot-melt-pressure-sensitive-adhesive/ Accessed: 2019-01-30
[18] J.H. Kang, R.G. Bryant, W.K. Wilkie, H.M. Wadsworth, P.D. Craven, M.K. Nehls and J.A. Vaughn. Simulated space environment effects on a candidate solar sail material. *NASA TP* 2017-219644.